Multi-IF-over-Fiber Based Mobile Fronthaul with Blind Linearization and Flexible Dispersion Induced Bandwidth Penalty Mitigation

Peixuan Li, Wei Pan, Long Huang, Xihua Zou, *Senior Member, IEEE*, Yan Pan, Qi Zhou, You-Wei Chen, Peng-Chun Peng, Siming Liu, Shuyi Shen and Gee-Kung Chang, *Fellow, IEEE, Fellow, OSA*

Abstract—The nonlinear degradations and chromatic dispersion induced bandwidth penalty are critical obstacles for implementing the analog radio-over-fiber (A-RoF) technique in future mobile fronthaul (MFH). In this paper, we propose an analog multiple intermediate-frequency-over-fiber (multi-IFoF) MFH system with blind linearity improvement and flexible dispersion-induced bandwidth penalty mitigation. The bias adjustment of a single-electrode driven dual-drive Mach-Zehnder modulator is used to compensate the bandwidth penalty ar\ising from the dispersion-induced power fading of fiber links in different lengths. This operation can increase the available bandwidth for the MFH system free of even-order intermodulation distortions (IMDs). At the receiver, a self-adaptive digital post-processing algorithm is introduced to blindly improve the linearity of the IFoF MFH system by suppressing the residual odd-order IMDs, with no need of training signals or prior knowledge of the transmission channel. In the proof-of-concept experiments, the transmission of 64-QAM-OFDM signals in 1 to 12 IF channels with a 500-MHz bandwidth has been demonstrated over standard single-mode fibers (SSMFs) of 20, 50 and 100 km. For the 50-km (or 100-km) SSMF, the bandwidth penalty for a broadband signal with a bandwidth of 4.5 GHz (or 2.5 GHz) is fully compensated. In addition, the proposed post-processing algorithm can significantly suppress the odd-order IMDs and thus improve the linearity by greater than 5.4 dB in terms of the input RF power range which acceptable error-vector-magnitude performance for the 64-QAM-OFDM signal.

Index Terms—IF over fiber, mobile fronthaul, external modulation, nonlinear distortion, dispersion-induced bandwidth penalty, digital signal post-processing.

Manuscript received XXX. This work was supported in part by the National Natural Science Foundation of China under grant (61775185), Sichuan Science and Technology Program (2018HH0002). (Corresponding author: Xihua Zou, email: zouxihua@swjtu.edu.cn)

P. Li, W. Pan, X. Zou and Y. Pan are with the Center for Information Photonics and Communications, School of Information Science and Technology, Southwest Jiaotong University, Chengdu 610031, China (P. Li, e-mail: lipeixuango@163.com; wpan@swjtu.edu.cn; zouxihua@swjtu.edu.cn; py_swjtu@my.swjtu.edu.cn).

L. Huang is with the National Laboratory of Microstructures, Nanjing University, Nanjing 210093, China, and also with the School of Engineering and Applied Sciences, Nanjing University, Nanjing 210093, China (e-mail: draghuang@gmail.com)

Q. Zhou, Y.-W. Chen, P.-C. Peng, S. Liu, S. Shen and G.-K. Chang are with the School of Electrical and Computer Engineering, Georgia Institute of Technology, Atlanta, GA 30308 USA (e-mail: qi.zhou@gatech.edu; ywchen77115@gmail.com; pcpeng@mail.ntut.edu.tw; siming.liu@ece.gatech.edu; ssyzoe@gatech.edu; geekung.chang@ece.gatech.edu)

I. INTRODUCTION

The centralized radio access network (C-RAN) is considered as an ▲ important architecture for the 5th generation (5G) mobile communication and beyond [1]. In the deployment of the advanced C-RAN, the mobile fronthaul (MFH) network is of significance to connect the central units (CUs) and distributed units (DUs) in Fronthaul II or DUs and remote radio units (RRUs) in Fronthaul I [2], [3]. Current MFH network employing digital interfaces (e.g., Common Public Radio Interface (CPRI) [4] and Open Base Station Architecture Initiative (OBSAI) [5]) accentuates the principal drawback of bandwidth inefficiency. Emerging 5G technologies like carrier aggregation (CA) and massive multiple-input and multiple-output (M-MIMO) are approaching growing fronthaul data rates, which will further intensify the exhausting bandwidth resources and drive new schemes for the MFH's evolution toward 5G and beyond. Among these efforts are BBU functional split [6], data compression [7], and analog intermediate frequency-over-fiber (IFoF) [8]. The IFoF technology has gained some traction owing to the promise of high spectral efficiency, low cost and multiservice compatibility. By combining the IFoF and frequency-division multiplexing (FDM) techniques, multiple IFs carrying individual mobile baseband signals can be aggregated in the frequency domain and transmitted in a single optical wavelength channel. In this way, low bandwidth efficiency of the MFH network can be resolved thanks to the analog signaling [9]-[13]. For instance, when the IFoF technology is applied, the required bandwidth for 59-Gb/s CPRI-equivalent data rate is only 1.5 GHz [9]. Consequently, high-capacity IFoF based MFHs network with CPRI-equivalent data rates as high as 190 Gb/s [10], 400 Gb/s [11] and even 1.032 Tb/s [12] have been demonstrated.

Nevertheless, the implementation of the analog IFoF in MFH as an enabling alternative for CPRI is hindered by two vital challenges. First, the impairments [e.g., the nonlinear intermodulation distortions (IMDs) attributable to the nonlinearities of the electrical amplifier, electrical to optical (E/O) and optical to electrical (O/E) conversions] will restrict the input power dynamic range of the IFoF MFH system. Especially, orthogonal frequency-division multiplexing (OFDM) signals are widely adopted in the MFH network for achieving higher spectral efficiency. The large number of subcarriers, continuously varying envelope, and high peak-to-average power ratio (PAPR) of OFDM would further worsen the nonlinear distortions (NLDs) problem [14]. On the other hand, Fig. 1 shows two potential deployment scenarios for the

C-RAN to meet different operators' requirements [30]. The IFoF transmission scheme here is employed for the Fronthaul I to connect the CU/DU and RRU. For the C-RAN system, the distance between the central office and the remote radio unit could be as long as 100 km [2]. In scenario (1), Fronthaul I can be implemented with a short fiber of several kilometers, as Fronthaul II in the next-generation fronthaul interface (NGFI) is expected to have an extended transmission distance ranging from 20 to 80 km [15]. However, in scenario (2), the IFoF-based Fronthaul I might be expected to reach a distance up to 100 km. Accordingly, the radiofrequency (RF) power fading arising from the chromatic dispersion of a long fiber link will seriously limit the available bandwidth of the MFH system.

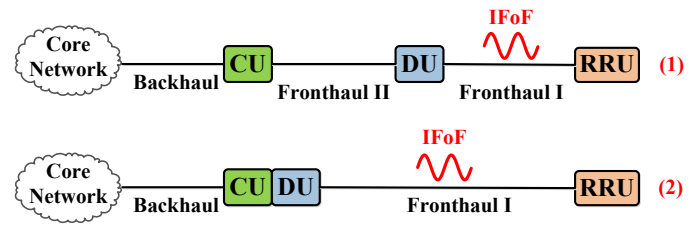


Fig. 1. Two potential deployment scenarios for the C-RAN, where the IFoF transmission scheme is employed for the Fronthaul I to connect the center unit (CU)/distributed unit (DU) and remote radio unit (RRU).

Many approaches have been proposed over the years to improve the linearity for the analog MFH network [16]-[27], wherein the digital linearization technology is used to provide an active, flexible and simple solution. Additionally, its inherent compatibility with IFoF-based MFH systems desiring digital-signal-processing (DSP)-assisted de-aggregation/aggregation [9]-[13] adds much coveted additional benefits. Consequently, a number of digital linearization schemes based on digital pre- or post-distortion have been proposed and have proven their usefulness in reducing NLDs both at baseband and RF frequencies [18]-[27]. However, all these techniques rely on training signals or prior knowledge of the transmission channel in order to derive equalization coefficients necessary for precisely compensating the NLDs. The training signals would increase the system overhead and reduce effective channel capacity. Also, the channel information acquired from one-time channel response probing cannot support these techniques in fast varying environments. Digital blind NLD mitigation methods for analog MFH, which are based on the calculation of adjacent channel leakage ratio (ACLR), have been released in [26], [27]. However, the proof-of-principle experiments only involve back-to-back (BtB) conditions; they are only applicable for transmitting signals with fixed center frequency and bandwidth, rather than with dynamic bandwidth allocation [28], as may be the case in software-defined channel allocations.

The chromatic dispersion of the fiber links typically leads to frequency-dependent RF power fading, such that the available flat RF bandwidth will be reduced, which is defined as the dispersion-induced bandwidth penalty in this paper. Methods such as parallel phase/intensity modulation (PM/IM) transmitter [12] and single sideband (SSB) modulation [15] can effectively overcome the dispersion induced power fading and mitigate the bandwidth penalty. However, these approaches feature either bulky in structure or lossy in RF power. Additionally, as well known, the even-order IMDs are usually located out of the signal

bandwidth and can be easily eliminated through filtering. Thus, the even-order IMDs can be ignored in order to reduce the complexity of algorithms [13], [16], [17], [22]-[27]. Generally, to circumvent the even-order IMDs, the signal to be transmitted is a bandpass one, of which the initial frequency is specified greater than its bandwidth to isolate the even-order IMDs. Then, an optical transmitter capable of mitigating the dispersion-induced bandwidth penalty for the MFH system free of even-order IMDs and while supporting power-efficient optical double-sideband modulation (DSB) with a compact structure is highly preferable.

In this paper, for the multiple IFoF-based MFH system free of even-order IMDs, we propose a novel signal processing scheme to achieve blind linearity improvement and flexible mitigation of dispersion induced bandwidth penalty. In the signal processing scheme, only one arm of a dual-drive Mach-Zehnder modulator (DDMZM) is driven with judicious biasing, to encode IF signal onto an optical carrier and an adaptive digital signal linearization algorithm is to post-processing the digitized received IF signal. The single-electrode driven DDMZM (SD-DDMZM) is employed to develop a simplified transmitter supporting optical DSB modulation. Its DC bias is dynamically adjusted to shift the peak of the frequency response to be aligned with the transmitted bandpass signal, for the purpose of dispersion-induced power fading compensation and available bandwidth increase under the scenarios of different flexible transmission distances. At the receiver, a self-adaptive digital post-processing algorithm with no need of training signals or transmission channel information feedback is used to alleviate the odd-order IMDs for the broadband signal centered at IF band. In the proof-of-concept experiments, broadband IF signals are generated via the aggregations of multiple 500-MHz IF channels (1, 5, 9, 12). In the IF channels, 64 quadrature amplitude modulation (64-OAM) OFDM signals are successfully transmitted over standard single-mode fibers (SSMFs) set at various discrete lengths 20, 50 and 100 km. Compensations of the RF power fading arising from the 50- and 100-km SSMFs are also demonstrated. Finally, for all of the investigated scenarios, the proposed post-processing algorithm shows excellent performance regarding the increment of input RF power range satisfying the error vector magnitude (EVM) limit for 64-QAM transmission. An improvement in the input power margin of more than 5.4 dB is achieved.

II. ARCHITECTURE OF PROPOSED MFH SYSTEM AND PRINCIPLE OF OPERATION

Figure 2(a) depicts the architecture of the proposed scheme for mitigating the nonlinear IMDs and chromatic dispersion effects (CDEs) in the multiple IFoF based MFH network. The basic framework for the point-to-point transmission originates from the MFH network presented in [11]. In the CU or DU, multiple digital baseband signals are carried by different IFs and multiplexed in the frequency domain through the DSP-based channel aggregation/de-aggregation techniques. By optically distributing these multiple analog IF signals to the RRU, bandwidth-efficient MFH network can be realized. We here use an external SD-DDMZM as the optical transmitter to relieve the dispersion induced bandwidth penalty. In the RRU, a digital self-adaptive NLD mitigation procedure is added before the channel de-aggregation. These linearized IF signals

are then de-aggregated to feed the antennas. It should be noted that only downlink transmission is shown in Fig. 2(a) and discussed in the rest of our paper, due to the similarity between the uplink and downlink transmission links.

To support multiple RRUs, the system could be similar to the passive optical network (PON) having optical line terminals (OLTs) and optical network units (ONUs). For the scenario of the long-reach network (up to 100 km), the shared fiber link should be as close to the ONUs as possible before splitting point to reduce the deployment cost. Hence, the distance differences from individual ONUs to the OLT are generally

short as compared to the shared fiber link, such that the CDE differences among ONUs are negligible. In this case, by using a single SD-DDMZM to mitigate the CDE of the long-reach fiber link, the time division multiplexing (TDM) PON architecture [29] should be capable of supporting a point-to-multipoint MFH network. As the variations of fiber distances from different ONUs to OLT cannot be ignored, wavelength division multiplexing (WDM) PON configuration having multiple optical transmitters for individual wavelengths could be considered [30].

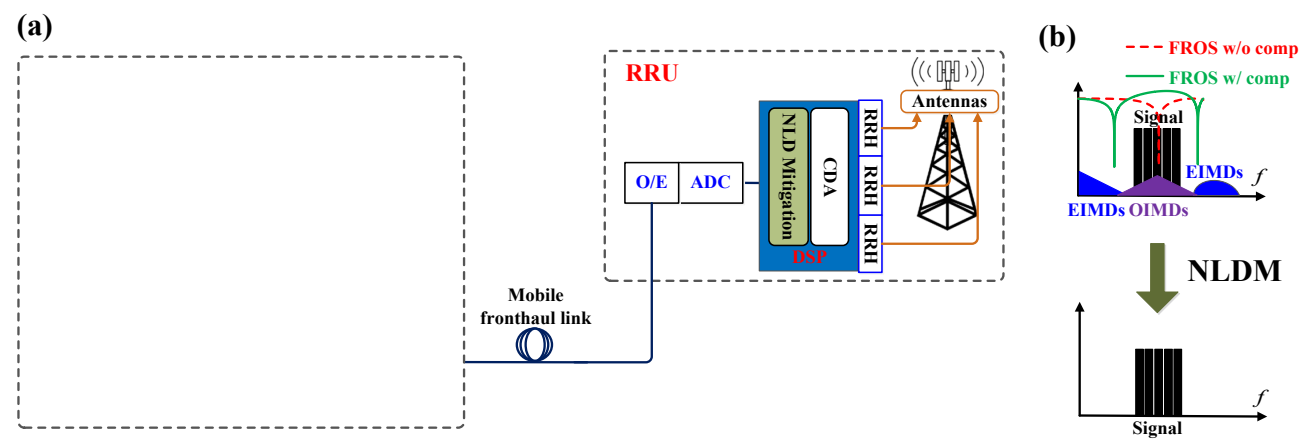


Fig. 2. (a) Architecture of the proposed multi-IFoF based MFH network. CU/DU: central unit/distribute unit; DSP: digital signal processing; CA: channel aggregation; CDA: channel de-aggregation; DAC: digital-to-analog converter; ADC: analog-to-digital converter; DS: downlink signal; US: uplink signal; NLD: nonlinear distortion; RRU: remote radio unit; RRH: remote radio head; LD: laser diode; DDMZM: dual-drive Mach-Zehnder modulator; PD: photodetector. (b) Operational principle demonstrated by the evolution of the electrical spectra for the received electrical signal. OIMDs: odd-order intermodulation distortions. EIMDs: even-order intermodulation distortions. FROS: frequency response of system the system with compensation (solid blue line) and without compensation (dashed red line).

A. CDEs Mitigation Using SD-DDMZM

As shown in Fig. 2(a) and (b), to move the even-order IMDs out of the signal bandwidth and acquire the sub-carrier channels, the initial frequency of the transmitted IF signal is spectrally shifted away from the baseband. A single inexpensive photodetector used in the direct detection of a broadband IFoF signal will suffer from the reduced bandwidth due to frequency-dependent power fading caused by the CDE in fiber. A simple transmitter for implementing double-sideband (DSB) modulation is introduced here, by using a single SD-DDMZM. Only one RF port of the SD-DDMZM is driven by the RF signal while the other is left open. In this way, the peak of frequency response from the baseband to IF can be shifted to ensure that the recovered odd-order IFoF signal is little affected by frequency-dependent RF fading during fiber transmission, as depicted on the top of Fig. 2(b). Then, the bandwidth of the flat bandpass range (i.e., the equivalent bandwidth of IF signal) can be increased. According to the discussions in [31], the dispersion-induced frequency-dependent RF power fading can be approximately expressed as

$$P_{\Omega} \propto \sin(\frac{\pi L D \lambda^2}{c} f^2) + \sin(\frac{\pi L D \lambda^2}{c} f^2 - \theta),$$
 (1)

where Ω is the angular frequency of the input RF signal, D is the fiber dispersion coefficient, L is fiber length, λ and c are the wavelength and speed of light, respectively. θ is the phase difference between two arms of DDMZM, which can be controlled by tuning the DC bias. In contrast, the power fading

in conventional intensity modulation (CIM) based transmission link is governed by [12]

$$P_{\Omega} \propto \cos(\frac{\pi L D \lambda^2}{c} f^2)$$
. (2)

From (1), the RF power fading mitigation scheme proposed here can be considered as being equivalent to a tunable microwave filter where the DC bias shifts the peaks of its frequency response to any specific frequency, f_c .

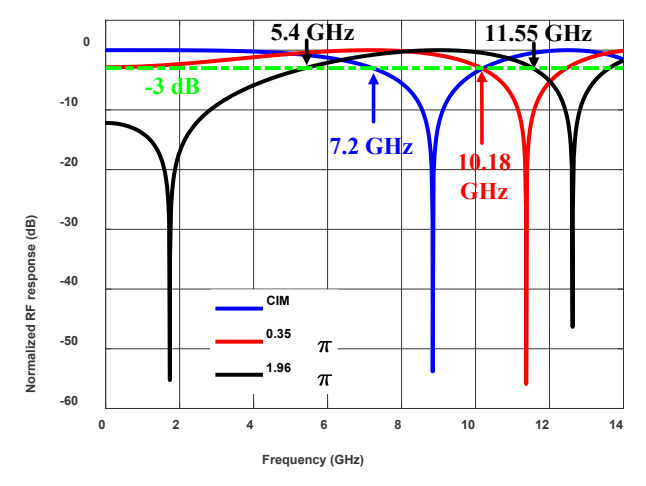


Fig. 3. Calculated frequency responses for system based on the conventional intensity modulation (CIM) (blue line), and the SD-DDMZM with θ =0.35 π (red line) and θ =1.96 π (black line)

For instance, for a 50-km SSMF with a chromatic dispersion coefficient (D) of 16 ps/km/nm, Fig 3 shows the calculated frequency responses of the transmission links using CIM and SD-DDMZM. The existence of power fading at specific frequency would cause bandwidth penalty to the MFH system. For the CIM, the 3-dB cutoff frequency is less than 7.2 GHz. However, it has been extended from 7.2 to 10.18 GHz, when replacing the CIM with the SD-DDMZM for θ =0.35 π . Since the even-order IMDs-free bandwidth of the transmitted signal should fall below half of its highest frequency, the maximum available 3-dB bandwidth will increase from 3.6 to 5.09 GHz. In another example, $\theta=1.96\pi$ is specified and frequency-dependent power fading of the system is characterized with an equivalent bandpass response from 5.4 to 11.55 GHz. For a given bandpass signal with an upper limit of 11.55 GHz, it is evident that the maximum available bandwidth can reach 5.77 GHz for the even-order IMDs circumvention. Therefore, for a given length of the fiber link between CU/DU and RRU, the SD-DDMZM-based transmitter can mitigate the CDEs induced bandwidth penalty and thus to enable extended transmission distance for the MFH network considering even-order IMDs elimination.

B. NLDs Mitigation Using Digital Self-adaptive Post-processing

Due to the limited optical power and short fiber link, the NLDs caused by the E/O and O/E conversions become the dominant factor for the performance degradation of the MFH network. In a fiber link using an external electro-optic modulator, the two-tone signal analysis can be used to characterize the nonlinear behavior. A two-tone input signal centered at angular frequencies $\Omega_c \pm \Delta \Omega$, is applied, which is expressed by

$$S(t) = V(t)\cos(\Delta\Omega t)\cos(\Omega t), \qquad (3)$$

where V(t) denotes the amplitude. Then the optical field at the output of the SD-DDMZM can be written as

$$E_1 = \sqrt{P_{in} \gamma} e^{j\omega_c t} \left(e^{jB(t)\cos\Omega_c t} + e^{j\theta} \right), \tag{4}$$

where

$$B(t) = \pi \cdot \frac{V(t)\cos(\Delta\Omega t)}{V_{\pi}}.$$
 (5)

 P_{in} and ω_c are the power and angular frequency of continuous-wave (CW) optical carrier. θ is the phase difference between two arms of DDMZM, which is introduced by the DC bias. V_{π} and γ are the half-wave voltage and insertion loss of the DDMZM, respectively. After fiber transmission, the electrical field of the optical signal in the fiber before entering the PD can be represented as

$$E_{2} = \sqrt{P_{in}\gamma G} e^{j\omega_{c}t} \{ [J_{0}(B(t)) + e^{j\theta}] e^{j\phi_{0}} + jJ_{1}(B(t))(e^{j\Omega_{c}t}e^{j\phi_{1}} + e^{-j\Omega_{c}t}e^{j\phi_{2}}) \},$$
(6)

where G is the gain of the fiber link, $J_n(\cdot)$ is the nth-order Bessel function of the first kind, and φ_i (i = 0,1,2) are the additional dispersion-induced phases. At the output of the PD, the recovered signal can be derived as

$$i \approx \Re P_{in} \gamma G\{ [J_0(B(t))J_1(B(t))\cos(\Omega_c t + \sigma)\sin(\chi) + J_1(B(t))\sin(\chi - \theta)\cos(\Omega_c t + \sigma) \},$$
(7)

where \Re is the responsivity of PD, σ represents the constant phase value, and $\chi = \varphi_1 + \varphi_2 - 2\varphi_0 = (\pi L D \lambda^2 f^2 / c)$ determines the dispersion-induced power fading. It is noted that only the components at Ω_c are considered. Expanding (7) in a Taylor series [32], we obtain

$$i \approx \Re P_{in} \gamma G \cos(\Omega_c t) \left\{ \underbrace{\frac{B(t)}{2} [\sin(\chi) + \sin(\chi - \theta)]}_{Signal} - B^3(t) \left[\frac{3}{16} \sin(\chi) + \frac{1}{16} \sin(\chi - \theta) \right] \right\} + B^5(t) \left[\underbrace{\frac{11}{384} \sin(\chi) + \frac{1}{192} \sin(\chi - \theta) \right] - \dots}_{Nonlinearity}$$

$$(8)$$

Hence, as shown in (8), the recovered signal is accompanied by components of third and fifth powers of B(t), previously referred to as odd-order IMD components. Assuming that the signal is centered at the peak of the passband response of the proposed system, it is reasonable to have

$$m_1 = \sin(\chi) + \sin(\chi - \theta) = 2. \tag{9}$$

When NLDs higher than 5th-order are ignored, (8) can be rewritten as

 $i \approx \Re P_{in} \gamma G \cos(\Omega_c t) [B(t) - m_3 B^3(t) + m_5 B^5(t)],$ (10a) where $B^3(t)$ and $B^5(t)$ contribute to the third-order and fifth-order IMDs (IMD3 and IMD5) and

$$m_3 = \frac{3}{16}\sin(\chi) + \frac{1}{16}\sin(\chi - \theta),$$
 (10b)

$$m_5 = \frac{11}{384}\sin(\chi) + \frac{1}{192}\sin(\chi - \theta)$$
. (10c)

Generally, to mitigate the NLDs, a high-degree polynomial is employed,

$$i_{out} = \alpha_1 i + \alpha_2 i^2 + \alpha_3 i^3 + ... + \alpha_n i^n$$
, (11)

where $\alpha_n(n=1,2,3...)$ are the polynomial coefficients. By substituting (10a) into (11), the linearized output is derived as

$$i_{out} = a_1 i + a_3 i^3$$

$$= \cos(\Omega_c t) \{ a_1 \underbrace{\Re P_{in} \gamma G[B(t) - m_3 B^3(t) + m_5 B^5(t)]}_{i} \}.$$

$$+ a_3 \underbrace{\frac{3(\Re P_{in} \gamma G)^3}{4} [B^3(t) - 3m_3 B^5(t)]}_{3} \}$$

Since the IMD3 is the most detrimental factor in the analog transmission system, the third-order polynomial is employed, while the even-order IMDs (e.g., a_2i^2) and NLDs higher than 5th-order are ignored. By neglecting the minor contribution of $B^5(t)$, the linearization condition becomes

$$\frac{3(\Re P_{in}\gamma G)^2}{4m_3} = \frac{a_1}{a_3} \,. \tag{13}$$

To acquire the coefficients, α_1 and α_3 , many parameters including the power of optical carrier, the gain of fiber link, and the responsivity of PD need to be precisely measured. Also, m_3 is highly frequency-dependent. The use of training sequence could be an effective method to estimate the channel parameters. However, for a dynamic system, the training process should be implemented repeatedly to adaptively compensate the NLDs, leading to a significant increase of the system overhead.

In [33], we proposed a self-adaptive digital post-processing algorithm to improve the linearity of the microwave photonic downconversion system. This algorithm is based on the specific characteristic of analog fiber-optic system that the intermodulation component, IMD3, is approximately phase shifted by $\sim \pi$ with respect to the fundamental subcarrier. By checking (8)-(12), we can get new relations as

$$m_1 = 2 \Rightarrow \sin(\chi) = \sin(\chi - \theta) = 1 \text{ and } m_3 > 0.$$
 (14)

Accordingly, from (8), the condition that IMD3 and fundamental signals have opposite signs is still consistent with our system. Then, an apparent characteristic can be observed in (12); that is, the IMD3 and IMD5 components of i (i.e., X_1') and that of i^3 (i.e., X_3') are out of phase in π . Hence, as we discussed in [33], X_1' and X_3' can be distinguished from other kinds of signals in the frequency domain by comparing the sign of i and i^3 after performing FFT. Eventually, the maximum value of the modulus of $\alpha_1 X_1' + \alpha_3 X_3'$ is monitored to derive α_1 and α_3 adaptively.

In addition, note that the algorithm in [33] is only applicable for the multi-tone sinusoidal signals in BtB transmission situation. For the MFH network, broadband baseband or IF signal and the transmission in fiber links should be taken into account. In this case, several issues should be addressed. First, (9) is not applicable for all frequency components for a broadband signal. However, it can be concluded that if $|m_1| \ge 1$, the condition, m_1 and m_3 have the same sign, is in accordance with (14). Thus, if the bandwidth of the broadband signal is less than the 3-dB passband of the system, the algorithm discussed above is feasible over its entire frequency spectrum. Second, in [33], the linearization coefficients are dynamically adjusted to minimize the maximum value of the modulus of $\alpha_1 X_1' + \alpha_3 X_3'$. The feasibility of this method is just verified in a narrowband system with multi-tone sinusoidal signals, where the NLDs are quite simple. However, for the IFoF MFH employing multiple bands of multicarrier OFDM signals being transmitted in a long fiber link, the resultant intra or inter band NLDs are much more complicated. In this case, besides the odd-order IMDs (mainly IMD3, IMD5), X'_1 and X'_1 may contain other kinds of signals having the highest amplitude, and thus minimizing the maximum value of $|\alpha_1 X_1' + \alpha_3 X_3'|$ cannot guarantee an effective suppression of odd-order IMDs. To relieve this problem, the average value of $|\alpha_1 X_1' + \alpha_3 X_3'|$, rather than the maximum value, is introduced here as the monitoring criterion, to facilitate the applications of broadband multiple IF OFDM signals.

Furthermore, as in [25], [26], the information concerning the center frequency and bandwidth of the signal is essential in [33] to get rid of the impact of other kind of noises such as the even-order IMDs. However, in the following experiments, we will verify that this information is not required in our proposal, making the proposed algorithm more suitable for systems with dynamic bandwidth allocation. Finally, according to the theoretical analysis above, the out-of-phase relationship between the odd-order IMD components of i and those of i^n holds for any odd power of i (i^n , n = 3,5,7...). Therefore, the effects of odd powers of i greater than 3 are explored experimentally to improve the performance of the proposed digital NLD mitigation (DNM) method.

Figure 4 illustrates the flow diagram of the proposed digital NLD post-compensation algorithm. First, the input signal i and its odd power i^n are converted into the frequency domain via fast Fourier transformation (FFT). Afterwards, we compare the FFT values of i and i^n which are centered at the same frequency point, to check whether they are opposite in sign. If YES, their values are stored in X_1' and X_3' respectively. Thus, assume that the frequency-domain odd-order IMD signals of i and i^n are found out. Then, α_1 is set as 1 to further simplify the algorithm and the rest of our task is to search the optimized coefficients α_3 to minimize the average value of $\left|X_1' + \alpha_3 X_3'\right|$. Both the constant-step searching algorithm [33] and the steepest descent algorithm [27] can be used here to obtain α_3 . In the end, the linearized output is given by $i_{out} = i + a_3 i^n$.

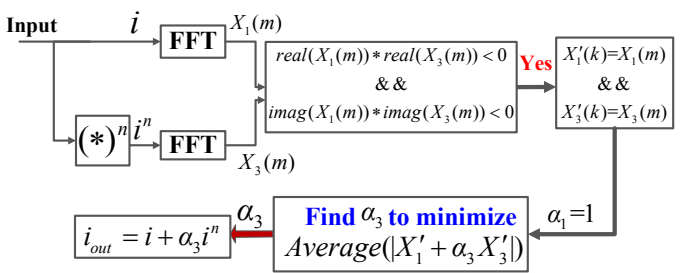


Fig. 4. Flow diagram of the proposed NLD mitigation algorithm. FFT: fast Fourier transformation.

The proposed digital post-processing algorithm outperforms by simple implementation and self-adaptability to the dynamic environment in the absence of the training process or any prior channel knowledge. Nevertheless, there exist several shortcomings. The first one is the transformation between the frequency and time domains, making this algorithm hardware unfriendly real-time processing. Nevertheless. FFT/IFFT-based channel aggregation and de-aggregation technique has been discussed in [9], [11] and believed to be a powerful tool for the bandwidth-efficient and low-latency MFH network. In this case, inserting our algorithm into the frequency-domain channel de-aggregation seems very appealing. On the other hand, the proposed algorithm may not be feasible when the signal power is so small that the performance becomes noise-limited rather than IMD-limited. This issue was also discussed in [26], [27]. A potential solution is to add a power monitor module to examine the power level of the input RF signal. If the power level of input signal beyond a

specific power threshold, the power monitor module can generate an enabling signal to activate the DNM operation; otherwise, the operation remains off. In the following experiments, we will verify that in a system having fixed nonlinear physical components including electrical amplifiers, E/O and O/E devices, the specific power threshold obtained from a preliminary test can be applicable for various scenarios of which the number of IF channels and transmission distances are different.

III. EXPERIMENTS AND DISCUSSIONS

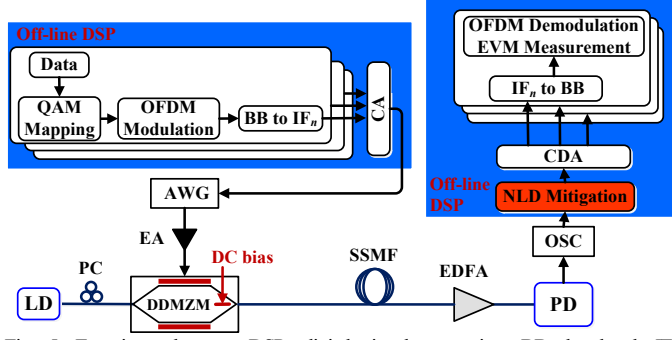


Fig. 5. Experimental setup. DSP: digital signal processing; BB: baseband; IF: intermediate frequency; CA: channel aggregation; AWG: arbitrary waveform generator; EA: electrical amplifier. PC: polarization controller; SSMF: standard single-mode fiber; EDFA: Erbium-doped fiber amplifier, PD: photodetector, OSC: real-time oscilloscope; NLD: nonlinear distortion; CDA: channel de-aggregation.

Several experiments are performed based on the setup shown in Fig. 5. The baseband signals to be transmitted are the 64-QAM OFDM signals with an FFT size of 2048 points, wherein 1000 subcarriers are allocated for data loading. Since the subcarrier spacing is specified as 500 kHz, each baseband OFDM signal occupies a bandwidth of 500 MHz. Subsequently, these baseband signals are upconverted to different IF subbands, which are aggregated with a guard-band spacing of 12 MHz. This multiple IFs based signal is generated by an off-line DSP and then fed into the high-speed arbitrary waveform generator (AWG, Keysight M9502A) running at 32 GSa/s. The AWG output is boosted by an electrical amplifier (EA) and applied to one of the RF input ports of the DDMZM (Fujitsu FTM7937EZ), which has a 40-GHz bandwidth and a 1.8 V half-wave voltage. After the SSMF transmission, an Erbium-doped fiber amplifier (EDFA) is used to compensate for the loss of the long-distance fiber transmission (up to 100 km). Noted that, in our experimental demonstrations, we install the EDFA at the receiver site to achieve an optimized received optical power for the employed PD without an embedded transimpedance amplifier (TIA). Generally, it is preferable to have the EDFA located at the transmitter site to simplify the RRU, and an integrated TIA-PD or an electric low noise amplifier could replace the EDFA at the receiver site.

The recovered electrical signal at the output of the PD is captured by the 40 GSa/s real-time oscilloscope (OSC, Keysight DSOZ254A). Off-line DSP including NLD mitigation, channel de-aggregation, OFDM demodulation and EVM measurement is then implemented to evaluate the performance of the system.

A. 20-km SSMF Link

To test the feasibility of the proposed DNM algorithm over a 20km SSMF link, we use a single 500-MHz 64-QAM OFDM signal centered at 6.8 GHz. Due to the relatively short fiber link, the DC bias is adjusted to minimize the nonlinearity of system. When the peak-to-peak voltage (V_{PP}) of the signal from AWG is 650 mV and the received optical power level before PD is 3 dBm, the NLDs are analyzed. Figure 6(a) displays the spectra of received signals with and without the DNM, when the observing bandwidth is 12 GHz. Here, the order of power n for the input signal to the DNM algorithm is 5, and the constant-step searching method is used to obtain the linearization coefficient α_3 . As can be seen in Fig. 6(a), the odd-order IMDs close to the desired signal is effectively suppressed by the proposed algorithm, while the even-order IMDs still remain. An over 10-dB improvement of signal-to-noise ratio (SNR) can be observed in Fig. 6(b). Also, compared to Fig. 6(c), much clearer constellation is observed in Fig. 6(d), resulting from the decrease of EVM from 15.19% to 3.87%. It is noted that the DNM algorithm works at a blind circumstance, without prior training or a prior knowledge of channel response. In addition, the center frequency and bandwidth of transmitted signals which are essential in [25], [26], [33] for ACLR calculation or even-order IMDs elimination are blind to us here.

In the same experiment, the EVM performances of the proposed system versus different input RF power levels are investigated without and with DNM having different values of n (n=3,5,7,9), as shown in Fig. 7. When the power of input RF signal exceeds -10 dBm, the proposed DNM can improve the EVM of the system. A significant increase to the highest input signal power satisfying the 8% EVM threshold, specified by the 3rd Generation Partnership Project (3GPP), is achieved for the 64-QAM signal. Also, as discussed in the last paragraph of Section II, the DNM is expected to degrade the system performance, rather than improve its performance, when the input RF signal is weak. Since this drawback can be overcome through the on-off switching of the DNM, only the highest input signal power satisfying the EVM requirement for 64-QAM signal concerns our experimental discussions.

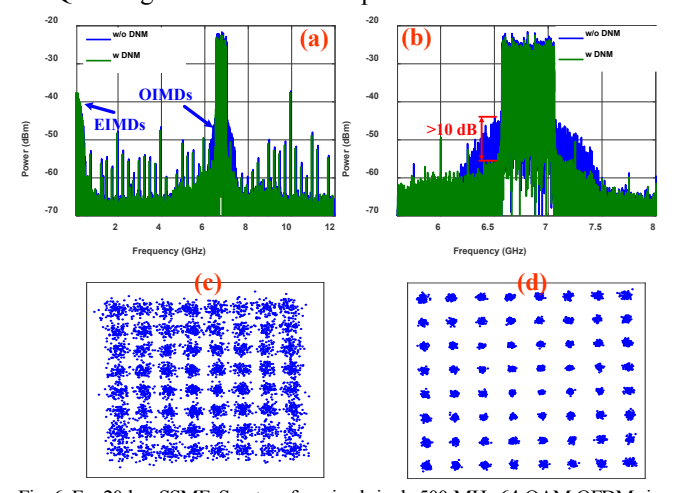


Fig. 6. For 20-km SSMF, Spectra of received single 500-MHz 64-QAM OFDM signals with/without DNM with observing bandwidths of 12 GHz (a) and 3 GHz (b). Constellations of the demodulated signals before (c) and after (d) DNM.

More importantly, from Fig. 7, we can conclude that the value of n is not restricted as 3, and that the DNM algorithm is equally effective for higher values of n (e.g. n=5,7,9). Especially, when the RF input power is relatively high, the DNM with a higher value of n outperforms that with n=3. Typically, the increment of input RF power range satisfying the 3GPP-specified EVM performance for the 64-QAM modulation rises from 4.8 dB (n=3) to 5.4 dB (n=5).

With the same length of SSMF, we also explore the case of channel packing in which different numbers of IF channels are aggregated. Thus, the aggregates of 5, 9 and 12 500-MHz 64-QAM OFDM signals are transmitted in three individual experiments. The received signal power spectrum for each IF aggregate is shown in Figs. 8(a1)-(c1) with and without DNM. Each IF frequency band is designed to circumvent the even-order IMDs. The total RF power for each of the three IFoF aggregates is set at 0.25 dBm and n for the DNM algorithm is 5. Assisted by the proposed DNM, the SNR of each received IF aggregate is improved. Although the degree of improvement in SNR performance differs for each aggregate, the resultant SNRs of their linearized output can reach the same level of ~ 26

dB. Thus, Figs. 8(a2)-(c2) suggest that in the absence of DNM, all IF channels fail to meet the 3GPP EVM specification. Fortunately, the DNM is employed and capable of achieving EVM-compliant levels in all IF channels.

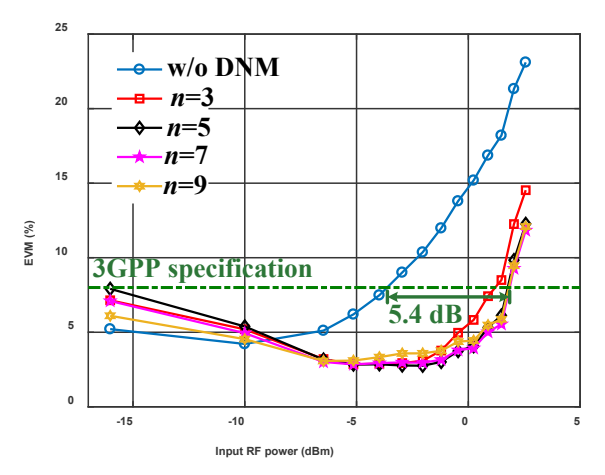


Fig. 7. When the fiber length is 20 km, (a) EVM performances of proposed system versus different input RF power without and with DNM possessing different values of $\,n\,$

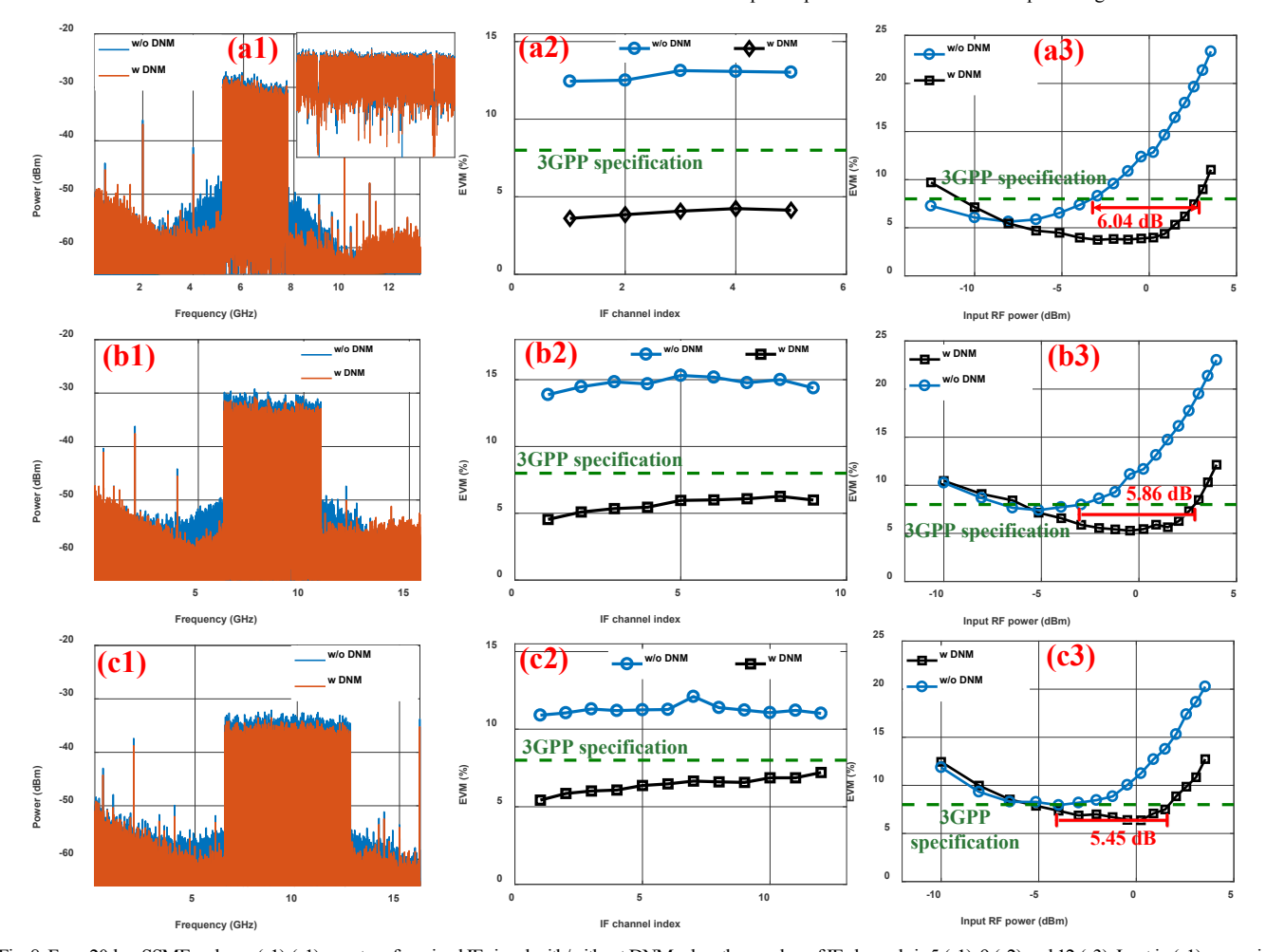


Fig. 8. For a 20-km SSMF, column (a1)-(c1): spectra of received IF signal with/without DNM when the number of IF channels is 5 (a1), 9 (a2) and 12 (a3). Inset in (a1): zoom-in view of spectra within a span of 700 MHz. Column (a2)-(c2): measured EVMs for all IF carriers with/without DNM in cases of 5 (a2), 9 (b2), and 12 (c2) IF channels. Column (a3)-(c3): measured average EVMs of all IF carriers versus different input RF power without/with DNM for 5 (c1), 9 (c2), 12 (c3) IF channels.

Additionally, in Figs. 8(a3)-(c3), the measured average EVMs of all IF carriers as a function of input RF power are demonstrated. Assisted by the proposed DNM algorithm, the

input RF power range is significantly improved by an approximately identical level in all the three cases, while satisfying the EVM requirement for the 64-OAM signal.

Hence, the self-adaptability of the proposed algorithm to various scenarios is verified by our experiments. On the other hand, the 6-GHz signal shown in Fig. 8(c1) consisting of 12 IF channels has reached the bandwidth limit of the used EA, while the CPRI-equivalent data rate is as high as \sim 368.6 Gb/s. This 368.6 Gb/s data rate is calculated as follows: 12 (IF channel) × 2 (IQ) × 30.72 × 500/20 (baseband sampling rate) × 15 (resolution) × 16/15 (CPRI overhead) × 10/8 (8b/10b coding) Mb/s. See references [11], [12].

B. 50 and 100-km SSMF Links

Next, longer fiber links will be taken into consideration. A 4.5-GHz signal with an aggregate power level of -2 dBm, originates from the aggregation of nine 500-MHz 64-QAM OFDM signals. The nine aggregated channels are firstly injected to the system with a 50-km SSMF link. The IF frequency bands range from 5 GHz to 9.55 GHz to avoid even-order IMDs. As shown in Fig. 9(a), if the bias voltage on the DDMZM is maintained at the same value as that for the 20-km fiber link, the fiber chromatic dispersion will cause frequency-dependent power fading to the high-frequency components of the transmitted IF signal and induce bandwidth penalty. Without any power compensation, except for the first IF channel, other IF channels cannot satisfy the EVM requirement for 64-QAM modulation [see Fig. 9(b)]. In our system, this issue can be easily relieved by changing the DC bias of the DDMZM. By adjusting the DC bias, the peak of the frequency response of the system can be shifted to a higher frequency and hence to compensate the power fading of the transmitted signal. Consequently, as can be seen in Fig. 9(b), by using the SD-DDMZM based power fading compensation and proposed DNM algorithm, the EVMs of the IF channels from 2 to 12 are significantly improved to reach the 3GPP specified EVM threshold for the 64-QAM signal.

Then, the length of fiber link is extended to 100 km. The number of 500-MHz IF channels decreases to five to ensure an acceptable SNR for the 100-km system. Thus a ~2.5 GHz IF signal centered at 6.8 GHz is applied to the system. As shown in Figs. 9(c) and 9(d), the signal spectrum is seriously distorted in the presence of dispersion-induced power fading such that the EVM of the received signal degrades. With the assistance of power fading compensation and the proposed DNM algorithm, the desired EVM-compliant levels in all the IF channels are obtained.

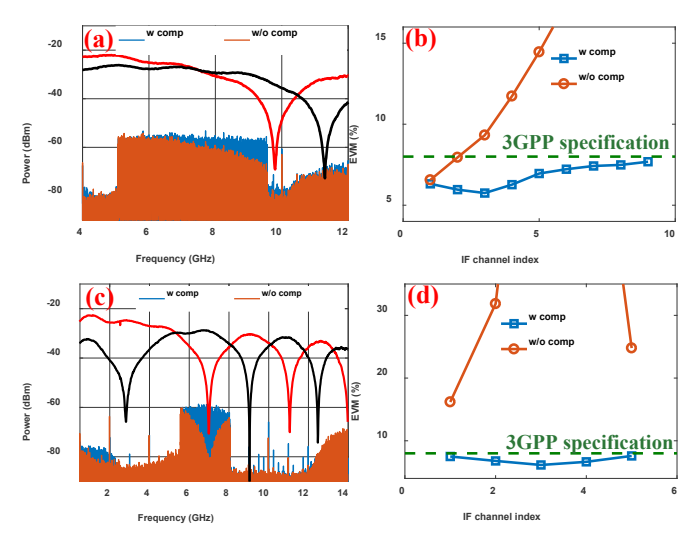


Fig. 9. Spectra of received signals when using (a) 50-km and (c) 100-km fiber links. The black line represents the frequency responses of system with power fading compensation, while the red line denotes the frequency response in the absence of power fading compensation. With proposed DNM algorithm, measured EVMs for all IF carriers with/without power fading compensation for (b) 50-km and (d) 100-km fiber links.

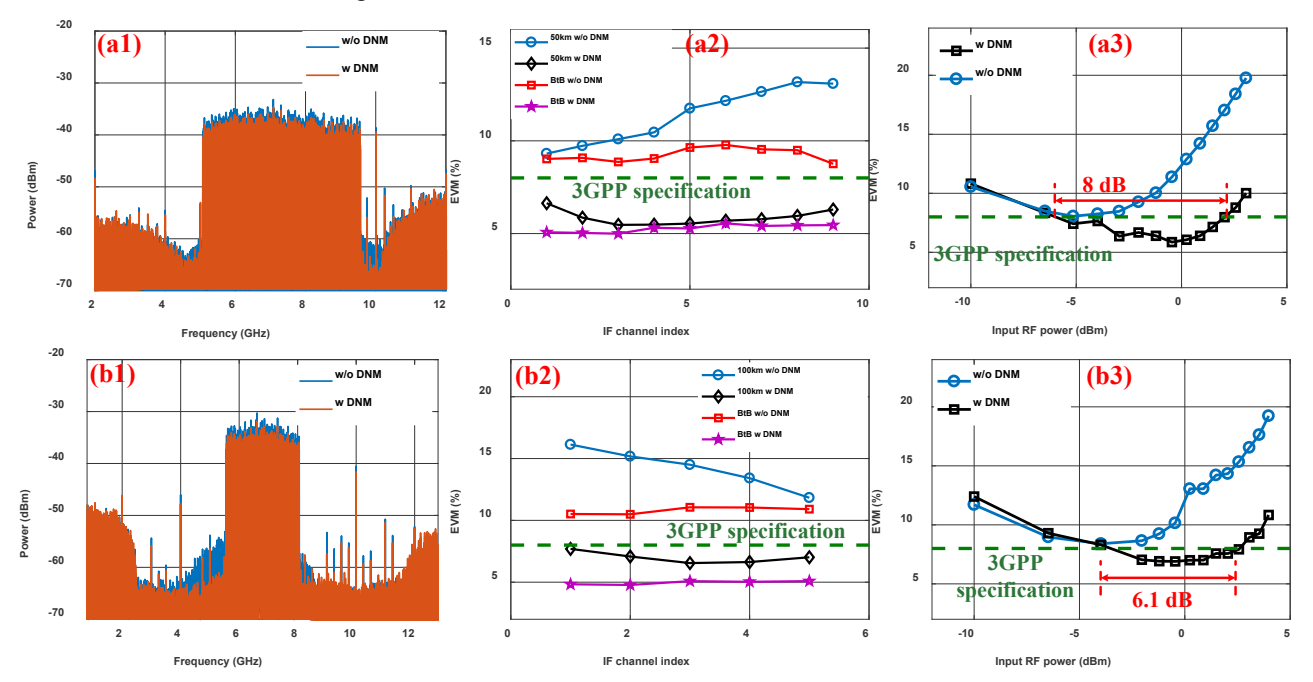


Fig. 10. Spectra of received signals with/without DNM for the (a1) 50-km and (b1) 100-km (b1) SSMF links. Measured EVMs for all IF carriers with/without DNM under different lengths of SSMFs, (a2) for 50 km, (b2) for 100 km. Measured average EVMs of all IF carriers versus different input RF power without/with DNM for the cases of 50-km (a3) and 100-km (b3) SSMFs.

The feasibility of the proposed DNM algorithm for 50-km and 100-km fiber links is further verified. The input RF power is 1.48 dBm, and the received optical power is 3 dBm and n=5. Figures 10(a1) and (b1) show the spectra of the received signal with and without DNM, respectively. Using the DNM, the odd-order IMDs suppression is observed for both 50-km and 100-km SSMF cases. On the other hand, obvious amplitude asymmetries in the upper and lower odd-order IMD components can be spotted in Figs. 10(a1) and (b1). As predicted in (4), the compensation of dispersion-induced power fading is achieved by controlling the modulation chirp. Thus, this phenomenon might be mainly caused by the interaction between fiber dispersion and modulation chirp. Therefore, as can be seen in Figs. 10(a2) and (b2), compared with the BtB situation, the EVMs of the system before DNM processing are degraded as the IF channel index increases (50 km) or decreases (100 km). Nevertheless, for these two cases, when the DNM is employed, both the upper and lower odd-order IMD components are effectively eliminated, leading not only to improvements in EVM performance for all IF channels, but also to the distinct reduction in the EVM discrepancy between them, shown in Figs. 10(a2) and (b2).

Noted that, after the DNM processing, the EVM difference between the 100-km and BtB transmissions [Fig. 10 (b2)] is larger than that between the 50-km and BtB transmissions [Fig. 10 (a2)]. A possible reason might be that the system noise induced after the 100-km fiber transmission is higher than that in the 50-km case. Hence, when the IMD signals are effectively suppressed, the 100-km system would be alternatively limited by the relative high system noise, leading to a worse EVM performance, compared with that of the BtB case. Additionally, the average EVMs of all IF channels are measured for both cases and demonstrated in Figs. 10(a3) and (b3). In the absence of the proposed DNM algorithm, all the input RF power levels cannot reach the EVM threshold of the 64-QAM signal. While using the DNM, long-distance transmissions of these signals are realized, and the range of input RF power easily straddles the required EVM threshold by 8 dB and 6.1 dB margins, respectively.

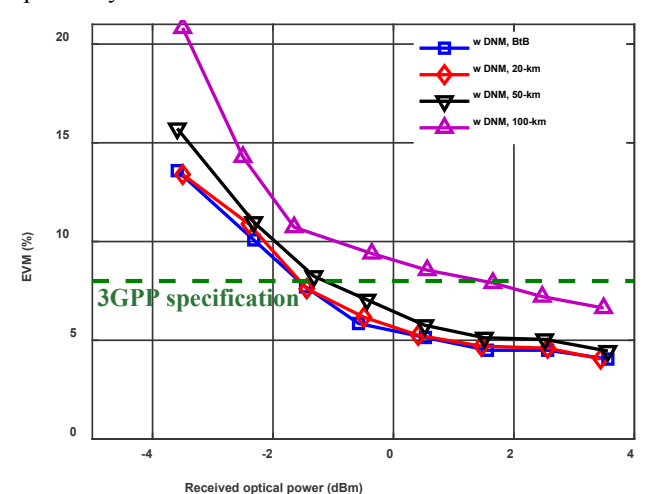


Fig. 11. Average EVM of all IF channels versus received optical power for 20, 50 and 100-km fiber links.

Moreover, from Fig. 7, a power threshold of around -8 dBm to activate the use of the DNM can be observed. Obviously, it is

also applicable for the cases shown in Figs. 8(a3)-(c3) and Figs. 10(a3)-(b3), of which the number of IF bands and transmission distances are different.

Finally, in Fig. 11, we demonstrate the EVM performance of the system by adjusting the received optical power for different transmission distances. For all the cases considered here, the aggregated signal comprises five 500-MHz 64-QAM OFDM signals, all of which have the same power level. The average EVM of all IF channels after DNM processing is used to evaluate the system performance. As revealed in Fig. 11, negligible power penalty is incurred over 20-km fiber transmission. For the 50-km and 100-km links, the power penalties for fulfilling the 8% EVM threshold are estimated to be ~ 0.5 and ~ 3.1 dB, respectively. In addition, the used EDFA can provide a fixed gain of ~28 dB and the output optical powers from DDMZM for 20, 50 and 100-km links are approximate 2.27, 3.3, and 2.25 dBm, respectively. Since the minimum received optical power levels to meet the EVM threshold are -1.8, -1.75 and 1.3 dB for 20, 50 and 100-km cases, the achieved link loss budgets are calculated as 32.07, 33.05 and 28.95 dB, respectively.

IV. CONCLUSION

We have designed and experimentally implemented a novel solution to overcome the problems of nonlinearity and CDEs for the analog multi-IFoF MFH network. When only the odd-order IMDs (primarily IMD3 and IMD5) which are typically overlapping with the transmitted signal are considered, a simple blind digital NLD post-processing algorithm for improving the linearity of the A-RoF system is theoretically analyzed and experimentally verified. This proposed DNM algorithm is successfully implemented for diverse application scenarios, including different number of IF channels (from 1 to 12), different transmission distances (20, 50 and 100 km) and even non-constant DDMZM bias conditions. More importantly, this DNM algorithm requires neither prior knowledge of transmission system nor training signals making it particularly suitable for fast-varying channel conditions with remarkably low additional overhead. An SD-DDMZM based optical transmitter is introduced to mitigate the signal bandwidth limitation arising from the chromatic dispersion in SSMFs and the use of even-order IMDs-free bandpass signals. By combining the power fading compensation and the DNM algorithm, CPRI-equivalent data rates of 276.5-Gb/s and 153.6-Gb/s over 50-km and 100-km SSMFs have been demonstrated with high spectral efficiency. This proposed method is expected to offer a viable alternative for achieving high input dynamic range but no overhead cost and for providing flexibility in bandwidth allocation and transmission distance adjustment in the MFH network.

REFERENCES

- [1] China Mobile Research Institute, "C-RAN: The road towards green RAN," Whitepaper v. 2.6, Sep. 2013.
- [2] I. Chih-Lin and J. Huang, "RAN revolution with NGFI (xHaul) for 5G," in Optical Fiber Commun. Conf. and Exhibition (OFC), March 2017, pp. 1-4
- [3] G.-K. Chang and P.-C. Peng, "Grand Challenges of Fiber Wireless Convergence for 5G Mobile Data Communications [Invited]," in *Proc. OECC*, Jul. 2018
- [4] Common Public Radio Interface (CPRI), CPRI Specification Version 6.1, 2014.
- [5] Open Base Station Architecture Initiative (OBSAI), OBSAI Specification RP3 Version 4.2, 2010.

- [6] J. Kani, J. Terada, K. Suzuki, and A. Otaka, "Solutions for future mobile fronthaul and access-network convergence," *J. Lightw. Technol.*, vol. 35, no. 3, pp. 527–534, Feb. 2017.
- [7] M. Xu, et al., "Key technologies for next-generation digital RoF mobile front-haul with statistical data compression and multiband modulation," *J. Lightw. Technol.*, vol. 35, no. 17, pp. 3671-3679, 2017.
- [8] C. Liu, et al., "A novel multi-service small-cell cloud radio access network for mobile backhaul and computing based on radio-over-fiber technologies," *J. Lightw. Technol.*, vol. 31, no. 17, pp. 2869–2875, Sep. 2013.
- [9] X. Liu, H. Zeng, N. Chand, and F. Effenberger, "Experimental demonstration of high-throughput low-latency mobile fronthaul supporting 48 20-MHz LTE signals with 59-Gb/s CPRI-equivalent rate and 2-μs processing latency," in *European Conf. Opt. Commun.*, Sep. 2015, paper We 4.4.3.
- [10] P. T. Dat, A. Kanno, N. Yamamoto, and T. Kawanishi, "190-Gb/s CPRI equivalent rate fiber-wireless mobile fronthaul for simultaneous transmission of LTE-A and f-OFDM signals," in *Proc. 42nd Eur. Conf. Opt. Commun.*, Sep. 2016, Paper W.4.P1.SC7.71
- [11] X. Liu, H. Zeng, N. Chand, and F. Effenberger, "Efficient mobile fronthaul via DSP-based channel aggregation," *J. Lightw. Technol.*, vol. 34, no. 6, pp. 1556–1564, Mar. 2016.
- [12] S. Ishimura, A. Bekkali, K. Tanaka, K. Nishimura, and M. Suzuki, "1.032-Tb/s CPRI-equivalent rate IF-over-fiber transmission using a parallel IM/PM transmitter for high-capacity mobile fronthaul links," *J. Lightw. Technol.*, vol. 36, no. 8, pp. 1478–1484, Apr. 2018.
- [13] M. Sung, et al., "Demonstration of IFoF-based mobile fronthaul in 5G prototype with 28-GHz millimeter wave," *J. Lightw. Technol.*, vol. 36, no. 2, pp. 601–609, Jan. 2018.
- [14] D. Dardari, V. Tralli, and A. Vaccari, "A theoretical characterization of nonlinear distortion effects in OFDM systems," *IEEE Trans. Commun.*, vol. 48, no. 10, pp. 1755-1764, Oct. 2000.
- [15] S. Shen, et al. "Spectrum-efficient 50-Gbps long-range optical access over 85-km SSMF via DML using windowed OFDM supporting quasi-gapless asynchronous multiband transmission," in *Optical Fiber Commun. Conf. and Exhibition (OFC)*, March 2018, paper M2B.5.
- [16] B. Hraimel, et al., "Performance enhancement of an OFDM ultra-wideband transmission-over-fiber link using a linearized mixed polarization single-drive x-cut Mach-Zehnder modulator," *IEEE Trans. Microw. Theory Techn.*, vol. 60, no. 10, pp. 3328-3338, Oct. 2012.
- [17] C. Han, S. Cho, H. S. Chung, J. H. Lee, "Linearity improvement of it modulated multi-IF-over-fibre LTE-A mobile fronthaul link using shunt diode predistorter," in *European Conf. Opt. Commun.*, Sep. 2015, paper We.4.4.4.
- [18] J. Zhang, et al., "Memory polynomial digital pre-distortion for linearity improvement of directly modulated multi-IF-over-fiber LTE mobile fronthaul," in *Optical Fiber Commun. Conf. and Exhibition (OFC)*, March 2016, paper Tu2B.3.
- [19] Z. Jia, et al., "Experimental demonstration of PDM-32QAM single-carrier 400G over 1200-km transmission enabled by training-assisted pre-equalization and look-up table," in *Optical Fiber Commun. Conf. and Exhibition (OFC)*, March 2016, paper Tu3A.4.
- [20] Y. Wang, J. Yu and N. Chi, "Demonstration of 4x128-Gb/s DFT-S OFDM signal transmission over 320-km SMF with IM/DD," *IEEE Photon. J.*, vol. 8, no. 2, article 7903209, 2016.
- [21] S. Liu, et al., "A multilevel artificial neural network nonlinear equalizer for millimeter-wave mobile fronthaul systems," *J. Lightwave Technol.*, vol. 35, no. 20, pp. 4406–4417, Oct. 2017.
- [22] Y. Pei et al., "Complexity-reduced digital predistortion for subcarrier multiplexed radio over fiber systems transmitting sparse multi-band RF signals," Opt. Express, vol. 21, no. 3, pp. 3708–3714, Feb. 2013.
- [23] C. Mateo, P. L. Carro, P. García-dúcar, J. de Mingo, and I. Salinas, "Radio-over-fiber linearization with optimized genetic algorithm CPWL model," Opt. Express, vol. 25, no. 4, pp. 3694–3708, Feb. 2017
- [24] X. Zhang, T. Liu, D. Shen, "Investigation of broadband digital predistortion for broadband radio over fiber transmission systems", *Opt. Commun.*, vol. 381, pp. 346-351, 2016.
- [25] C. Filipe, and A. Cartaxo. "Broad baseband nonlinear distortion mitigation using digital pre-and post-distortion in OFDM based WDM LR-PON." Opt. Express, vol. 23, no. 6, pp. 7062-7074, Mar. 2015.
- [26] Y. Pei, et al., "Digital multi-channel post-linearization for uplink in multi-band radio-over fiber systems," in *Optical Fiber Commun. Conf.* and Exhibition (OFC), March 2014, paper M3D.4.

- [27] H. J. Park, et al., "Distortion Mitigation in Multiband OFDM RoF Transmission Employing Blind Post Equalizer," *IEEE Photon. Technol. Lett.*, vol. 28, no. 23, pp. 2708–2711, Dec. 2016.
- [28] F. Liu, K. Zheng, W. Xiang, and H. Zhao, "Design and performance analysis of an uplink carrier aggregation scheme," *IEEE J. Sel. Areas Commun.*, vol. 32, no. 2, pp. 197–207, Feb. 2014.
- [29] T. Tashiro et al., "A novel DBA scheme for TDM-PON based mobile fronthaul," in *Proc. Opt. Fiber Commun. Conf. Exhib.*, Mar. 2014, Paper Tu3F.3.
- [30] J. S. Wey and J. Zhang, "Passive optical networks for 5G transport: technology and standards," *J. Light. Technol.*, to be published.
- [31] Y. Gao, et al., "An analog photonic link with compensation of dispersion-induced power fading," *IEEE Photon. Technol. Lett.*, vol. 27, no. 12, pp. 1301–1304, Jun. 2015.
- [32] A. Baricz, Generalized Bessel Functions of the First Kind. New York, NY, USA: Springer-Verlag, 1994.
- [33] Y. Pan et al., "Adaptive linearized microwave downconversion utilizing a single dual-electrode Mach–Zehnder modulator," *Opt. Lett.*, vol. 40, no. 11, pp. 2649–2652, Jun. 2015.
- [34] X. Yan, X. Zou, W. Pan, L. Yan, and J. Azaña, "Fully digital programmable optical frequency comb generation and application," *Opt. Lett.*, vol. 43, no.2, pp. 283-286, Jan. 2018.
- [35] X. Zou, et al., "Microwave Photonics for Featured Applications in High-Speed Railways: Communications, Detection, and Sensing," J. Light. Technol., vol. 36, no. 19, pp. 4337-4346, Oct. 2018.